International Journal of Mechanical Sciences 227 (2022) 107357

Contents lists available at ScienceDirect

International Journal of Mechanical Sciences

journal homepage: www.elsevier.com/locate/ijmecsci

Acoustics and vibrations in a complex piping network with pump startup–shutdown transients

Feroz Ahmed [a,*], Ian Eames [a], Alireza Azarbadegan [b], Emad Moeendarbary [a]

[a] Department of Mechanical Engineering, University College London, Torrington Place, London, WC1E 7JE, UK
[b] BP Exploration Operating Company Limited, Chertsey Road, Sunbury-on-Thames, Middlesex, TW16 7NL, UK

ARTICLE INFO

Keywords:
Reciprocating pump
Pulsation
Startup–shutdown
Transient flow
Piping network

ABSTRACT

Pump dynamic operational conditions result in extreme transient events that can enhance the response of piping networks. The predominant transients during rapid startup and shutdown are mainly studied for centrifugal pumps and are scarce for reciprocating pumps. Our study extends the conventional steady-state analysis to include the effect of reciprocating pump dynamic loading on pulsatile flow-induced acoustics and vibrations in a complex piping network. The forced response resulting from acoustical–structural coupling is assessed by utilising the one-dimensional multiphysics piping acoustic model and beam structural model. The network responses to pulsatile flows during dynamic pump loading (rapid start-up-shutdown events) are compared to the responses due to pulsatile flows during steady-state pump loading. With pump startup–shutdowns operations accompanied by pulsatile flows, the network response is the result of the combination of the transient and steady-state characteristics of plane acoustic waves and structural vibrations. The dynamic pump loading excites the fundamental, low-frequency acoustic eigenmode that causes transient loading of pipeline similar to reservoir–pipe–valve (RPV) systems.

1. Introduction

Hydraulic transients are major concerns in the industrial piping networks equipped with turbo-machineries, e.g., turbine-based hydro-electric power systems [1,2] and pumping systems (centrifugal [3–5] & positive-displacement [6] pumps). In oil pipelines driven by turbo-machinery pumps, a high pressure transient exists particularly due to rapid changes in the operational conditions of valves (e.g., rapid valve opening and closing [3,7,8]), pumps (e.g., startup–shutdown [4]), and speed changes [9]. In addition, the transient may also be produced as a result of power failure to the pump electric motors, pump failures [10,11], trips [12,13], or pipeline ruptures. The consequence of excessive piping vibration and cavitation associated with hydraulic transients is the loss in reliability & mechanical integrity (e.g., vibration-induced fatigue failures, instrument distortion and process efficiency), and process integrity (e.g., leaks, fire explosions, noise, environmental pollution, production downtime, human life, and safety) [14–16].

There is a large number of studies in the literature that highlight the effect of valve-induced [3,7,8,17,18] and pump-induced [4,19–21] transients in hydraulic systems. Typically, valve-induced pressure transients occur upon the closure of discharge valves within the reservoir–pipe–valve (RLV) systems [7,8,17,18]. The underlying mechanisms of the transient characteristics of pressure response in these systems are determined by the nature of the inlet and outlet flow conditions. The constant pressure at the reservoir-end and a zero flow at the valve-end (due to the rapid closure of the discharge valve) cause the water hammer phenomenon, one of the most widely studied in the RPV systems [17,18]. The valves in practical RPV systems are not always stationary but susceptible to vibrations. Pulsating (or oscillating or vibrating) motion of the valve coupled with the linear closure motion of the outlet valve leads to transient characteristics that differ from those of a typical water hammer condition.

The second most widely-studied transients in hydraulic piping systems are the pump-induced pressure transients, which are generated due to dynamic pump conditions, i.e., rapid pump startup [19,20], shutdown [21], or startup–shutdown events. The pump-induced transient pressure waves (which is predominantly studied for centrifugal pumps) is generated when the flow is constant (i.e., startup) or zero (i.e., shutdown) at the inlet-end and pressure is zero at the outlet-end. Interestingly, the transient characteristics associated with rapid pump startups and shutdowns are similar to those associated with valve openings and closings in reservoir–pipe–valve (RPV) systems, respectively [3–5].

The transients in hydraulic systems become severe, especially in pipeline systems with coupled pressure responses associated with rapid

* Corresponding author.
E-mail address: ucemfah@ucl.ac.uk (F. Ahmed).

https://doi.org/10.1016/j.ijmecsci.2022.107357
Received 2 March 2022; Received in revised form 21 March 2022; Accepted 11 May 2022
Available online 27 May 2022

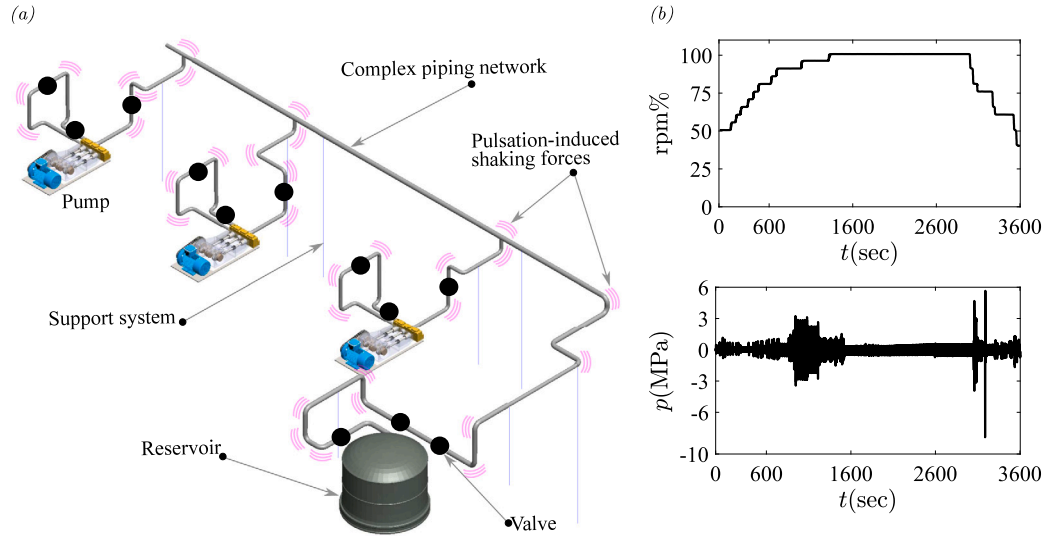

Fig. 1. (*a*) Schematic of an industrial complex piping network driven by three parallel high-pressure (multi-variable speed) reciprocating pumps. The pulsation-induced shaking forces at piping discontinuities or pipe fittings (bends, junctions, transitions, and valves) are highlighted. (*b*) Complex acoustic response in a piping network due to pump speed variations including startup–shutdown events. The response block consists of steady-state acoustic loading superimposed on transient loading.

pump operation and valve closure [22]. This is especially predominant in the practical hydraulic systems, where there is a network of branches with multiple inlet and outlet points [23]. The transient characteristics of acoustic waves in these systems are influenced by the dynamic interaction of pump and valve motions, as opposed to transient pressure waves in a single pipeline (e.g., rapid valve closure at the outlet of a pipeline, or pump startup and shutdown at the inlet) [24,25]. In order to understand how the pump-valve interactions occur, it is necessary to know the type of pump (i.e., centrifugal [26] or reciprocating [27]) and the conditions under which the pump operates (e.g., steady-state or startup–shutdown).

The two types of transient associated with reciprocating pump operations are (a) transient overshoot oscillation due to piston–chamber–valve interactions [28–32] and (b) transients due to dynamic pump conditions, i.e., rapid pump startup and shutdown. The piston–chamber–valve interaction (i.e., the motion of piston/plunger in a liquid chamber) in a high-pressure reciprocating pump generates distorted discharge pulsatile flow with jump-discontinuity in its profile (see the inset in Fig. 2*a* and the bottom panel in Fig. 4*a*) [31]. This discharge flow profile is accompanied by the transient overshoot, which is significantly weaker than the pulsation level [31]. The interplay between the reciprocating pump-induced pulsatile flow and piping acoustic standing waves generates steady-state pressure pulsation that propagates as a plane wave in a large piping network. In a complex piping network, the acoustic–structural coupling, not the pulsation, can generate large shaking forces at pipe discontinuities (bends, junctions, transitions, and valves) and small-bore connections (SBCs), resulting in vibration. The dynamic pump conditions are common during speed alterations and regular startup–shutdown operations [33]. The byproduct of these complex pump operational conditions is the extreme transient events, which enhance the acoustic–structural interaction through combined transient-steady-state pulsation-induced shaking loading (see Fig. 1). The transients caused by rapid pump operation (startup–shutdown) are mainly investigated for centrifugal pumps, and is scarce for reciprocating pumps [27]. As a consequence, the typical coupled acoustics and vibrations in piping networks are being studied using steady-state analysis (under constant pump speed operation) [23,34], where forced vibration can cause high-cycle fatigue (HCF). The transients are extremely important because, compared to steady-state pump speeds, the components of the piping system that are susceptible to resonance may be very different. Hence, the piping system can experience both high-cycle fatigue (HCF) and low-cycle fatigue (LCF) when subjected to transient loading conditions with pulsatile flows.

Our objective in this study is to investigate the response of a pipe network subjected to dynamic pump loading. We applied one-dimensional (1D) multiphysics models to a complex piping network under steady-state and dynamic pump loads in order to investigate various contributions towards the acoustic and vibration response of the piping network. The choice of the model system studied in this paper is justified in Section 2. This choice takes the problem outside the scope of an idealised academic model and more towards the type seen in industry. In doing so, we start to see an extraordinarily high level of complexity and some fundamental components that have a bearing on real problems. In Section 3, the multiphysical models and numerics are discussed to analyse plane acoustic wave propagation and piping structural vibration. Section 4 discusses results and discussion, covering pulsatile flow harmonics, eigenmodes, and acoustic and vibration responses.

2. Model system

We selected a particular model system so it can demonstrate the level of complexity involved in the energy sector while delivering mono-ethylene glycol (MEG). The system consists of a complex piping network connected with three parallel constant-speed high-pressure reciprocating pumps (see Fig. 1*a*). Parallel pumps are common in the industry to increase the volume flux through the piping networks [10,33,35–37]. We choose a five-chamber pump operating at elevated differential pressure $\Delta p (= p_d - p_s) = 77.6$ MPa (where p_d and p_s are discharge and suction pressure, respectively) with volumetric efficiency $\eta_v = 0.95$. Each pump at rated operational condition (i.e., point of best efficiency) with rated shaft frequency $f_{p,r} = 5.77$ Hz generates a large flux of discharge flow $Q_{m,r} = 6.11\times10^{-3}$ m^3/s with jump-discontinuity in its profile [31,38] (see the inset in Fig. 2*a*). The choice of pulsatile flow patterns is based on the manufacturer's pump data, and is discussed in [31]. The operational conditions of all pumps are kept the same, and the adverse interactions between the flow generated by two pumps, i.e., the time delay between the start of two pumps [31], are neglected.

We consider three types of pump operations that generate: (i) steady-state pulsatile flows (see Fig. 2*a*), (ii) rapid flow acceleration–deceleration simulating pump startup and shutdown events (see Fig. 2*b*) and (iii) rapid acceleration–deceleration with steady-state pulsatile

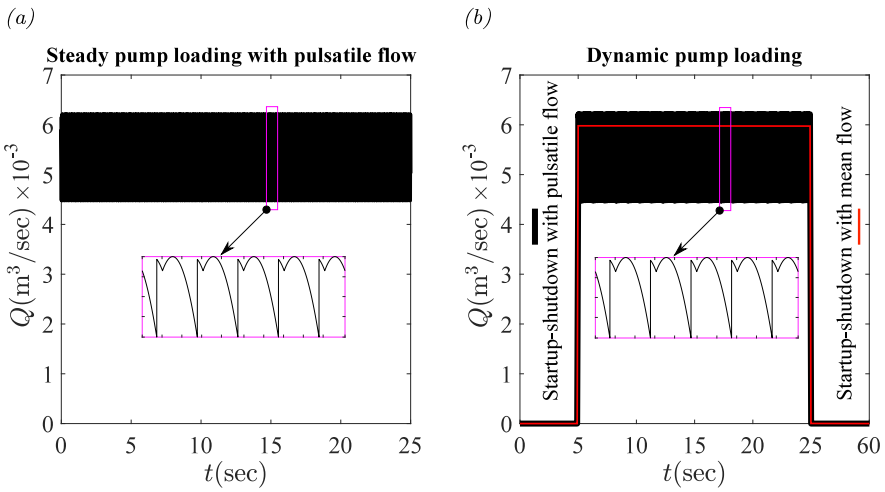

Fig. 2. Discharge flows from various pump loading operations — (*a*) steady-state pump loading with pulsatile flow, (*b*) dynamic pump loading (startup–shutdown) with mean flow and pulsatile flow. The inset in (*a*,*b*) describes the typical volume flux from a five-chamber pump ($\eta_v = 0.95$) under one-complete crank rotation.

flows (see Fig. 2*b*). The choice of stepped-pattern of the pump dynamic operation for pump startup (accelerating transient $\mathrm{d}Q/\mathrm{d}t > 0$) and shutdown (decelerating transient $\mathrm{d}Q/\mathrm{d}t < 0$) is based on the assumption of rapid transient pump dynamic operation (the worst-case scenario).

The steel pipe geometry (see Fig. 1*a*) contains large number of long pipes (with $L/D_o \gg 1$, where L is the pipe length and D_o the pipe outer diameter), thick pipes (with $D_o/T \simeq 4$, where D_o/T is the diameter-to-wall-thickness ratio), 90-degree curved pipes (with $R_c/D \simeq 2.3$ & 1.8 where R_c is the bend radius and D the pipe inner diameter), flow-thru junctions, and globe valves. The network is free from local cross-sectional ovalisation due to the presence of thick curved pipes. The weight of valves (each weighs 800 kg) are represented as spherical lumped masses. All support systems are assumed as clamped supports, which are represented as stiff elastic springs (with longitudinal spring constant of each support as 1×10^9 N/m). The choice of k is discussed in Section 4.2.1.

3. Mathematical model

Predicting plane acoustic wave propagation and the associated vibration response in a complex piping network requires multiphysics modelling approaches. The reduced-order coupled model consists of a zero-dimensional (0D) pump flow model, one-dimensional (1D) piping acoustic model, and one-dimensional (1D) piping structural model.

3.1. 0D Lumped parameter pump model

A reciprocating pump, driven by a common crankshaft, consists of multiple chambers with pistons (or plungers) and spring-loaded valves to create a unidirectional flow [39]. Based on the interaction mechanisms of piston kinematics, chamber fluid dynamics and valve dynamics, the reciprocating pump generates a wide range of discharge flow, ranging from smooth to distorted flow patterns [31]. There are several modelling methods to describe the flow from multi-chamber reciprocating pumps, including lumped parameter zero-dimensional (0D) model, distributed one-dimensional (1D) models [32] and distributed three-dimensional (3D) models. Here, we have adopted the lumped parameter approach to model the discharge flow (also used by [31,39]).

The discharge flow from a single reciprocating pump with multiple chambers is [31],

$$Q_a = \Big(1 - \big(\Delta p \beta r_v + S\big)\Big)(A_p l_p f_p N_c)\pi \frac{1}{N_c} \sum_{n=1}^{N_c} \sin\Big(2\pi f_p t + \frac{2\pi}{N_c}(n-1)\Big) \cdot F_n(t) \cdot G_n(t), \tag{1}$$

where Q_a is the actual effective flow, N_c the number of chambers, A_p the cross-sectional area of a chamber, l_p the stroke length, f_p the pump driving frequency, $\Delta p (= p_d - p_s)$ the differential pressure across discharge and suction valves, $\beta (= 1/K)$ the liquid's compressibility factor (where K is the bulk modulus), $r_v (= V_{cd}/V_p)$ the volume ratio, S the pump valve slip (or valve loss), $F(t)$ the phase cut, and $G(t)$ the effect of volumetric efficiency [31].

3.2. 1D Piping acoustic model

A one-dimensional (1D) model based on the relationship between volume flux (Q) and pressure (p) is used to analyse the flow of a slightly compressible (elastic) piping network. Since we are dealing with a liquid system, the change in fluid density is small, and we can appeal to a constant density acoustic model [31]. The 1D incompressible unsteady-state pipe flow equations (continuity and momentum) can be expressed as,

$$\begin{aligned} &\frac{\partial p}{\partial t} + \frac{\rho_0 a_0^2}{A}\frac{\partial Q}{\partial s} = 0, \\ &\frac{\partial Q}{\partial t} + \frac{A}{\rho_0}\frac{\partial p}{\partial s} + \frac{1}{2}\frac{\lambda^*}{D}\frac{|Q_0|Q}{A} = 0, \end{aligned} \tag{2}$$

where ρ_0 is the density of fluid at reference condition, s the distance along the centreline of a piping network, $D = \sqrt{4A/\pi}$ the pipe inner diameter, A the pipe cross-sectional area, and $Q_0 = Q_{m,r}$. The acoustic waves propagate along thick and stiff liquid-filled pipe with a constant wave speed $a_0 = 1480$ m/s [31].

The plane acoustic wave is attenuated as it propagates along a pipe network [18]. There are a wide range of parameters that influence the acoustic wave attenuation in liquid-filled piping networks: (a) nature of machine operations (steady-state [40,41], or transient-state), (b) nature of inflow conditions (steady, oscillatory [40] or pulsatile [41]), (c) nature of flow regimes (laminar [42], transitional or turbulent [43,44]), (d) nature of pipe wall conditions (smooth [43] or rough [44]), (e) nature of pipe elements (straight or pipe fittings [45]), and (f) nature of wall stiffness (compliant or rigid). The wall shear stress can be used to characterise the attenuation of plane acoustic waves in a piping network [42–44,46–49]. The instantaneous pipe wall shear stress (τ) for pulsatile turbulent pipe flows can be written as the combination of quasi-steady component (τ_s) and unsteady component (frequency-dependent wall shear stress) (τ_u) [50]. The mechanisms by which the energy is dissipated in pulsatile pipe flows are quite different from steady pipe flows. Based on the velocity profiles developed in pipes, one can ascertain the difference between τ_s and τ_u [51]. The two widely used 1D formulations [50,52] to model the unsteady component of wall

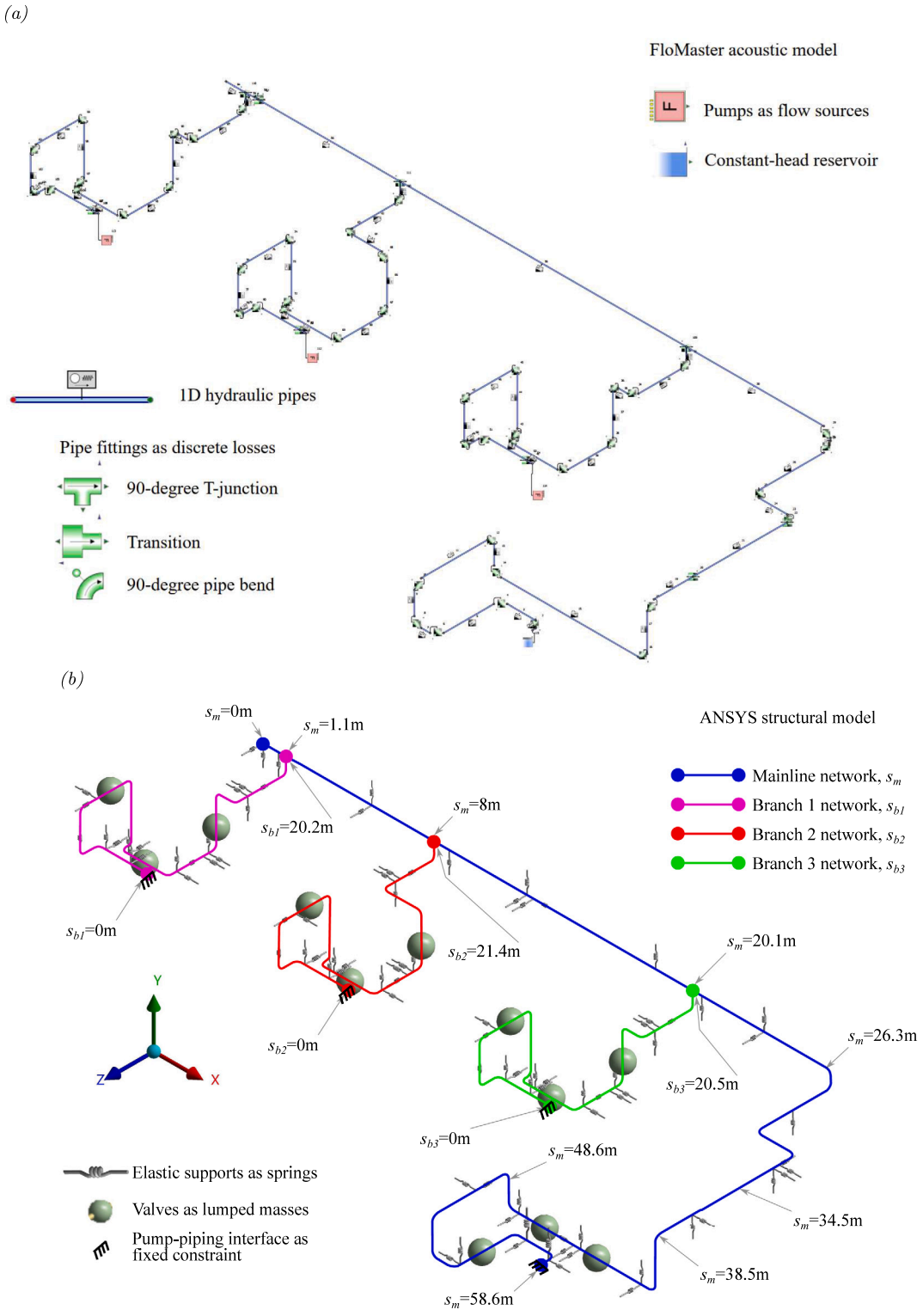

Fig. 3. Reduced-order multiphysics modelling of a three-dimensional liquid-filled complex piping network driven by three high-pressure reciprocating pumps. (*a*) FloMaster (MentorGraphics) piping plane acoustic wave propagation model. The piping acoustic network is modelled as 1D hydraulic pipe elements (cylindrical elastic pipes), the pipe fittings as discrete loss elements, the pumps as flow sources, and the reservoir as constant-head reservoir. (*b*) ANSYS Mechanical piping structural vibration model. The piping structural network is modelled as 1D line elements (PIPE289 and ELBOW290), the elastic clamped supports as spring elements (COMBIN14), the valves as lumped mass elements (MASS21) and pump-piping interface as rigidly-fixed constraints.

shear stress in pipelines are the weighting function-based (WFB) analytical models [42–44,46–49] and the instantaneous acceleration-based (IAB) empirical models [50,53].

Here, we have adopted the The IAB empirical shear stress model, which is more suitable than WAB for practical large-scale complex piping network [50]. Based on the Vitkovsky formulation [53] of

Brunone instanteneous acceleration-based (IAB) model, the empirical instantaneous friction factor (λ^*) can be written as the combination of quasi-steady and unsteady components as,

$$\lambda^* = \lambda + \frac{Ak\,D}{|Q_0|Q}\left(\frac{\partial Q}{\partial t} + a_0 \mathrm{sgn}(Q)\left|\frac{\partial Q}{\partial s}\right|\right), \tag{3}$$

where sgn is the signum function, λ the steady-state Darcy friction factor and k the unsteady-state friction coefficient.

3.2.1. Boundary conditions

The liquid-filled pipe network is a collection of nodes and pipe elements (see Fig. 3*a*), where p is continuous at nodes and the sum of the flux (Q) leading the node is equal to the flux arriving. The initial condition is that when the flow is quiescent and the outlet pressure is set and fixed. At pipe inlets (three pump locations), a time-varying Dirichlet (or essential) boundary condition is imposed as,

$$Q(0,t) = Q_0(t) \quad \text{and} \quad \frac{\mathrm{d}p(0,t)}{\mathrm{d}t} = 0, \qquad \text{for} \quad t > 0, \tag{4}$$

and at pipe outlet (constant head reservoir in Fig. 3*a*), the Neumann (or natural) boundary condition is $p = p_{\text{res}}$.

3.2.2. Acoustic-induced shaking force

The plane acoustic wave propagates and is attenuated along with a piping network due to friction losses, where the change in momentum flux and differential pressure across piping discontinuities leads to unsteady-state shaking forces. The bend force due to cross-wise components (secondary flow) is small compared to the contribution from the streamwise flow components [51]. Therefore, the net bend force experienced by the pipe bend associated with the streamwise flow components can be written as,

$$\boldsymbol{F} = -(p_i + \rho_0 u_i^2)A\hat{\boldsymbol{n}}_i - (p_o + \rho_0 u_o^2)A\hat{\boldsymbol{n}}_o \tag{5}$$

where $\hat{\boldsymbol{n}}_i (= (-1, 0))$ and $\hat{\boldsymbol{n}}_o (= (\cos\phi_b, -\sin\phi_b))$ are unit vectors normal to the pipe bend inlet and outlet, and $\phi_b (= 90°)$ is the bend angle. Similarly, the net force experienced by the tees is,

$$F = -(p_t + \rho_0 u_t^2)A\sin\phi_t, \tag{6}$$

where subscript t represents branch connection and $\phi_t (= 90°)$ is the branch angle.

3.3. 1D Piping structural vibration model

The piping structural vibration is described using a combination of stubby beam model ($L/D_o \geq 20$) and ($D_o/T \ll 20$) for straight pipes and thick plate model ($D_o/T \ll 1$) for curved pipes based on Timoshenko's analysis (or reduced first-order shear deformation beam theory) [54] and Reissner–Mindlin's analysis (or reduced first-order shear deformation plate theory) [55,56], respectively. Both theories consider rotatory inertia effect (due to twisting tendency in the 3D topological network) and transverse shear deformation effect (due to thick pipes). The flexural displacement field in Timoshenko beam theory and Reissner–Mindlin (toroidal) plate theory [56, Eq. 37] along the pipe is governed by,

$$\begin{aligned}
&\frac{\partial^2}{\partial s^2}\left(E\boldsymbol{I}(s)\frac{\partial^2 \mathbf{u}(s,t)}{\partial s^2}\right) + \rho_s A(s)\frac{\partial^2 \mathbf{u}(s,t)}{\partial t^2} \\
&\underbrace{-\rho_s \frac{\partial^2}{\partial s^2}\left(\boldsymbol{I}(s)\left(1 + \frac{E}{\kappa G}\right)\frac{\partial^2 \mathbf{u}(s,t)}{\partial t^2}\right)}_{\text{rotatory inertia effect (torsion related)}} \\
&+ \underbrace{\frac{\rho_s^2 \boldsymbol{I}(s)}{\kappa_b G}\frac{\partial^4 \mathbf{u}(s,t)}{\partial t^4} + \frac{E\mathbf{I}(s)}{\kappa_b AG}\frac{\partial^2 \boldsymbol{\mathcal{F}}(s,t)}{\partial s^2} - \frac{\rho_s \mathbf{I}(s)}{\kappa_b AG}\frac{\boldsymbol{\mathcal{F}}(s,t)}{\partial t^2}}_{\text{shear deformation effect (flexural related)}} = \boldsymbol{\mathcal{F}}_b(s,t)
\end{aligned} \tag{7}$$

and

$$\begin{aligned}
&\left(\boldsymbol{\nabla}^2 - \frac{\rho_s}{\kappa_p^2 G}\frac{\partial^2}{\partial t^2}\right)\left(D\boldsymbol{\nabla}^2 - \frac{\rho_s T^3}{12}\frac{\partial^2}{\partial t^2}\right)\boldsymbol{u} + \rho_s T\frac{\partial^2 \boldsymbol{u}}{\partial t^2} \\
&= \left(1 - \frac{D\boldsymbol{\nabla}^2}{\kappa_p^2 GT} + \frac{\rho_s T^2}{12\kappa_p^2 G}\frac{\partial^2}{\partial t^2}\right)\boldsymbol{\mathcal{F}}_p(\boldsymbol{x},t),
\end{aligned} \tag{8}$$

respectively. Here E and G are the Young's and shear modulus, respectively; $\boldsymbol{I}(= I_{xx}, I_{yy}, I_{zz})$ the area moment of inertia of pipe cross-section, ρ_s the pipe material density; D the flexural stiffness; T the pipe thickness, κ_b and κ_p the Timoshenko and plate shear correction factor, respectively; $\mathbf{x}(= x, y, z)$ the spatial coordinates; $\mathbf{u}(= u, v, w)$ the displacement field; $\boldsymbol{\nabla}(= \frac{\partial}{\partial x}, \frac{\partial}{\partial y}, \frac{\partial}{\partial z})$ the gradient; $\boldsymbol{\mathcal{F}}_b(s,t)$ the force per unit length on the beam; and $\boldsymbol{\mathcal{F}}_p(\boldsymbol{x},t)$ the moment and force distribution on the plate.

3.3.1. Support conditions

The piping network is physically supported and this is important for vibration study. The piping network is held at various points along the network using clamped supports, as shown in Fig. 3(*b*). It is usual practice to treat clamped pipes and their foundations as relatively stiff elements with a prescribed level of stiffness constant (k). The piping network is initially at rest, so we set initial condition ($t = 0$) in terms of both displacement and slope as constant,

$$\boldsymbol{u}(s,0) = 0, \qquad \frac{\partial \boldsymbol{u}(s,0)}{\partial s} = 0. \tag{9}$$

The pump sources and constant head reservoir are rigidly fixed (fully-constraint) (see Fig. 3*b*), so we set Dirichlet (or essential) boundary condition ($t > 0$) as,

$$\boldsymbol{u}(s_f,t) = 0, \qquad \frac{\partial \boldsymbol{u}(s_f,t)}{\partial s} = 0, \tag{10}$$

where $s_f\big(= (s_{b_1} = 0),\ (s_{b_2} = 0),\ (s_{b_3} = 0),\ \text{and}\ (s_m = 58.6\ \text{m})\big)$ are the fully-constraint locations in a piping network (see Fig. 3*b*).

3.3.2. Coupling between acoustic and mechanical model

In a long complex piping network, the acoustic waves propagate as plane fronts, leading to vibrations and cavitations when coupled with the structural modes. There has been much work conducted on the fluid–structure interaction (FSI) in a fluid-filled piping network [17,57–62]. For a liquid-filled piping network, FSI is typically classified into two types: (a) distributed FSI (Poisson and friction couplings), where the interaction acts along a pipe span in the form of wall motion, and (b) local FSI (junction and Bourdon couplings), where the interaction acts at specific locations, e.g., piping discontinuities (bends, tees, and valves) [59,63]. The Poisson coupling is a two-way-interaction process that leads to breathing or hoop mode of piping response (which is dominant in transient wave problems in reservoir–pipe–valve (RPV) systems [17]). In contrast, friction coupling due to the viscous effect at the pipe wall is a one-way-interaction process with the weakest contribution. The junction coupling [64] has the dominant contribution under the resonant condition at the point of discontinuity, which can result in unbalanced forces (shaking forces) in a network. The Bourdon coupling exerts its dominance when cross-sectional ovalisation occurs in thin pipes. The excitation mechanisms in local FSI is significantly larger than distributed FSI [63]. Since the piping network in this study is the collection of stubby pipe elements ($L/D_o \ll 1$ and $D_o/T \ll 1$) with a large number of stiff clamped supports, the junction coupling is the dominant driving mechanism, where the change in the flow direction around pipe discontinuities generates pulsation-induced shaking forces in the network.

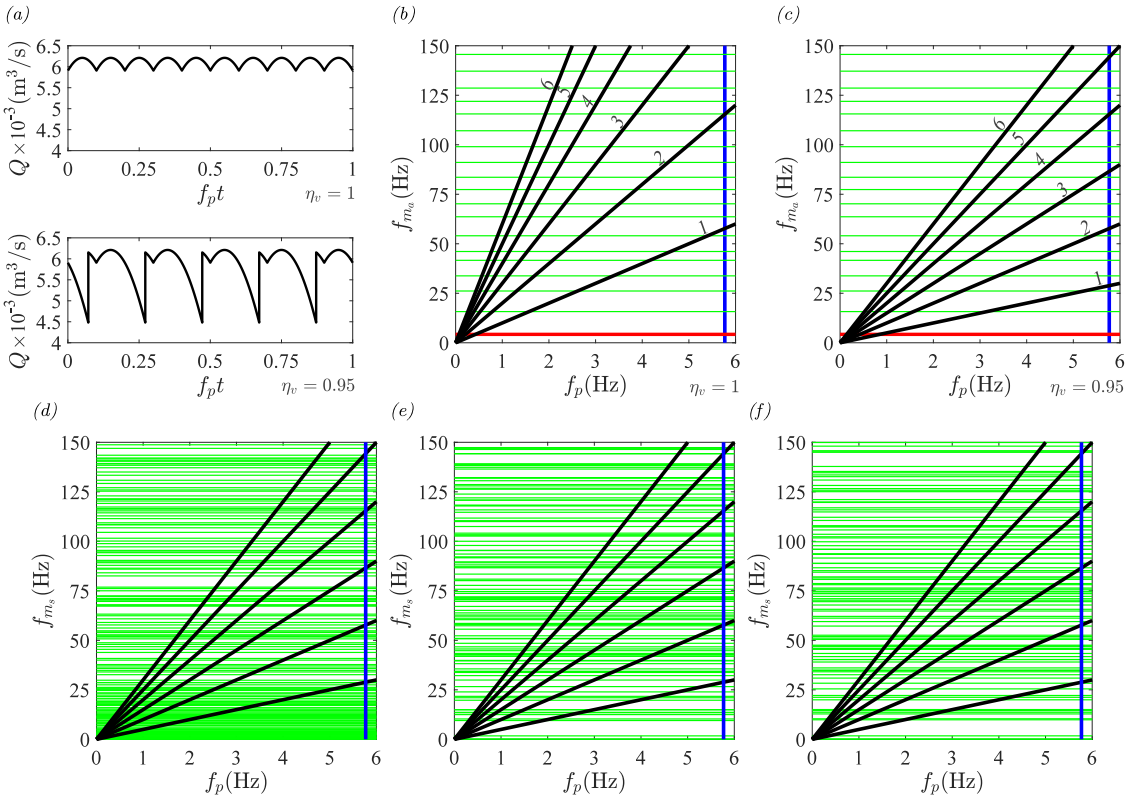

Fig. 4. (*a*) Discharge pulsatile flows from a single five-chamber reciprocating pump with volumetric efficiency $\eta_v = 1$ (top panel) and $\eta_v = 0.95$ (bottom panel) under one crank rotation. (*b,c*) Frequency-interference diagrams showing the interaction of pump speed ($f_{p,r}$), pulsatile flow harmonics (f_{m_p}), and acoustic eigenfrequencies (f_{m_a}). (d, e, f) Parametric variation of piping structural eigenfrequencies (f_{m_s}) at various longitudinal stiffness (k) of elastic clamped supports (see Fig. 3*b*) – (*d*) $k = 0$ N/m, (*e*) $k = 10^9$ N/m, and (*f*) $k = 10^{12}$ N/m. The eigenfrequencies (f_{m_a}: acoustical (b, c), f_{m_s}: structural (d, e, f)) of a piping network are plotted against pump frequencies (f_{m_p}). The thick-black lines (isolines) in (*b,c*) are the pulsatile flow harmonic order or excitation order (m_p) for flow with $\eta_v = 1$ and 0.95, respectively. Only the first-six excitation orders ($m_p = 1, 2, 3, 4, 5, 6$) are shown here. A thick-blue line represents the operating frequency ($f_{p,r} = 5.77$ Hz) of a single-acting five-chamber pump considered in this study. The horizontal lines (thin-green and thick-red) in (*b* and *c*) are the acoustic eigenfrequencies (f_{m_a}, estimated using FloMaster or COMSOL), while the horizontal lines (thin-green lines) in (d, e, f) are the structural eigenfrequencies (f_{m_s}, estimated using ANSYS). The thick-red lines in (b, c) are the fundamental acoustic eigenfrequency ($f_{m_a} = 4.3$ Hz) in a piping network.

3.4. Numerical implementation

The two widely-used coupled methods to solve the transient one-dimensional (1D) FSI in a liquid piping network are the frequency-domain methods (e.g., transfer matrix method (TMM) [65]) and time-domain methods (e.g., method of characteristics (MOC) [63], finite-element method (FEM) [66–68], MOC-FEM [69,70], and discrete-time transfer matrix method (DTTMM) [71]). Here, we have adopted the MOC-FEM method to solve the multiphysics piping acoustic and structural models.

The geometry of reduced-order coupled multiphysics interaction of a three-dimensional (3D) topological liquid-filled complex piping network (see Fig. 1*a*) was modelled using FloMaster (MentorGraphics) for plane acoustic wave propagation (see Fig. 3*a*) and ANSYS Mechanical for structural vibration (see Fig. 3*b*). As a first step, the 1D hydraulic flow network in FloMaster was generated by utilising FloEFD's CAD2FM functionality, which converts 3D piping CAD geometry into a 1D hydraulic network of straight pipes and discrete fittings. Furthermore, the 1D structural beam network in ANSYS Mechanical was developed by converting the CAD geometry into the 1D beam network of straight and curved pipes using the ANSYS SpaceClaim beam object functionality. In order to establish the structure of the piping network, a line-based modelling was used. Pipes were modelled using line elements (PIPE289 and ELBOW290), globe valves with lumped mass elements (MASS21), and clamped supports with spring elements (COMBIN14). The curved regions (and straight pipes near them) are modelled with ELBOW290, which is based on the thick plate theory of Reissner–Mindlin. As for straight pipes far from curved regions, PIPE289 is used, which is based on the Timoshenko stubby beam theory.

In the next step, the pipe flow equations (Eq. (2)) for a hydraulic network (see Fig. 3*a*) were solved by FloMaster implementing the method of characteristics (MOC). Since the piping network in this study is the collection of stiff and stubby pipe elements ($L/D_o \ll 1$ and $D_o/t \ll 1$), the junction coupling is the dominant driving mechanism, where the change in the flow direction around pipe discontinuities generates acoustic-induced (or pulsation-induced) shaking forces in the network. Next, the acoustic-induced forces were transferred to all structural pipe fittings using junction FSI coupling mechanism. The structural response of a piping network (Eqs. (7) and (8)) was then solved in ANSYS Mechanical using the finite-element method (FEM).

4. Piping dynamical response

A pump-piping system is susceptible to vibration-induced fatigue due to the interaction of pulsatile flow harmonics with acoustic eigenmodes and structural eigenmodes [31]. The type of pump loading can also affect the nature of acoustic–structural coupling in a piping network. The focus of this section is on the influence of pump dynamic effects (i.e., startup and shutdown) on acoustic wave propagation and structural vibration in a complex piping network.

4.1. Pulsatile flow harmonics

Fig. 4(*a*) shows the typical discharge volume flux (Q_a) generated from a single five-chamber reciprocating pump when the volumetric

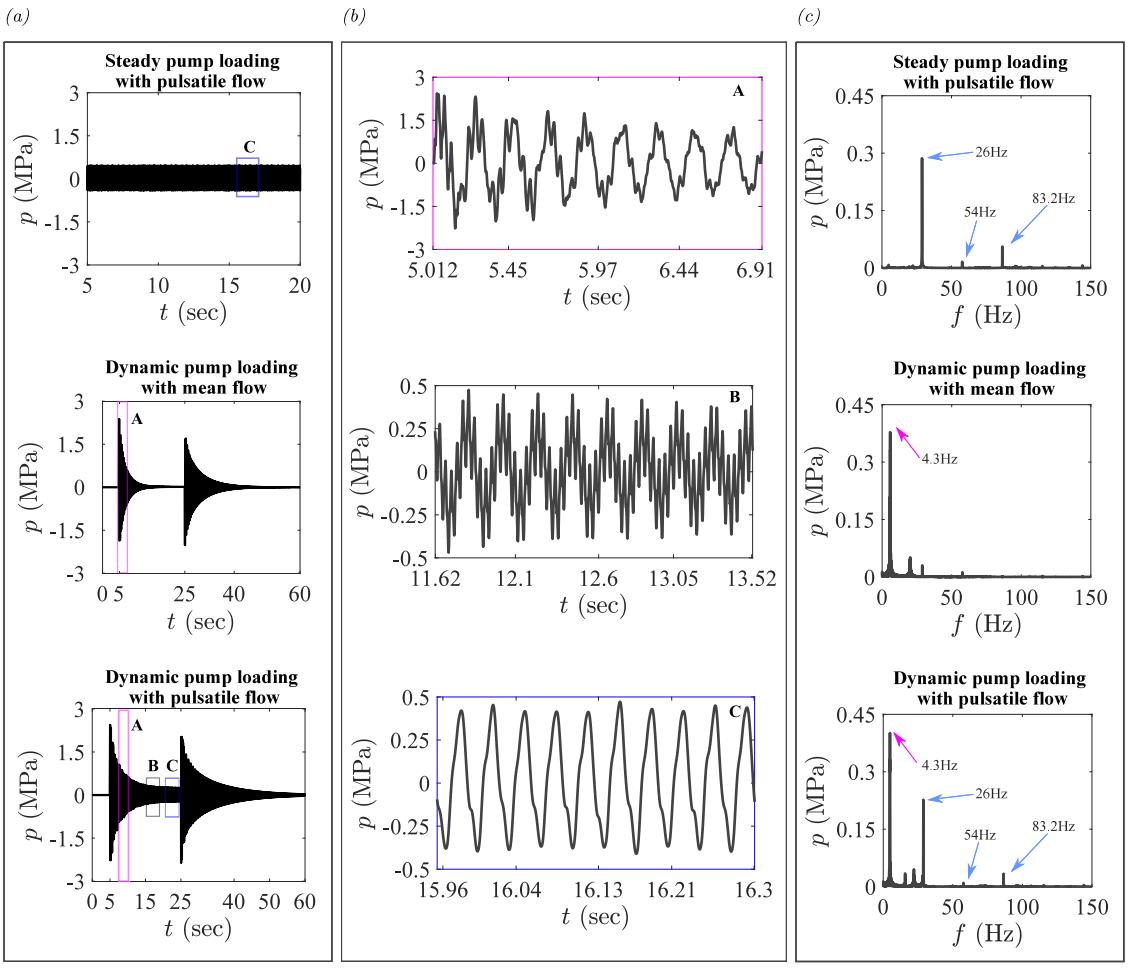

Fig. 5. Acoustic response in a piping network driven by three types of pump operations — steady-state pump loading with pulsatile flows, dynamic pump loading with mean flows and dynamic pump loading with pulsatile flows. The acoustic pressures captured at s_m = 26.3 m (see Fig. 3) are expressed in (*a*) time domain and (*c*) frequency domain. The snapshots in (*b*) highlight the zoomed-in regions of three critical features of non-stationary acoustic response due to dynamic pump loading with pulsatile flows. The critical features are low-frequency high-amplitude transient characteristics of pulsation (snapshot **A**), high-frequency low-amplitude steady-state characteristics of pulsation (snapshot **C**) and the coupled steady-state-transient characteristics of pulsation (snapshot **B**).

efficiency is $\eta_v = 1$ (top panel) and 0.95 (bottom panel). The shock-free flow at $\eta_v = 1$ is a theoretical (or ideal or geometric) pulsatile flow, when the occurrence of leakage while displacing fluid at low differential pressure Δp across pump is neglected [31,38]. Due to elevated differential pressure $\Delta p (= p_d - p_s) = 77.6$ MPa across the pump, liquid compressibility, and leakage (or slip) in the system, valve timing is delayed, thus reducing the volumetric efficiency of the system [31]. With $\eta_v = 0.95$, the pump generates a large flux of flow with a jump-discontinuity in its profile, resulting in a shock-jump pulsatile flow [31, 38]. In shock-free and shock-jump flows, the loading resulting from pulsatile flows occurs over a wide range of discrete forcing frequencies, known as pulsatile flow harmonics (f_{m_p}) that are multiples of pump frequency (f_p) (see Fig. 4*b,c*, respectively). Accordingly, the pulsatile flow harmonics of pumps with $\eta_v = 1$ and 0.95 can be calculated using $f_{m_p} = 2 \times m_p N_c f_p$ and $f_{m_p} = 1 \times m_p N_c f_p$, respectively [31].

4.2. Eigenmodes

An essential first step in the study of the acoustic–structural coupling in a piping system is to conduct network eigenmode analysis, either through the use of FloMaster or COMSOL (for acoustic propagation) and ANSYS (for structural vibration), in the absence of pump excitations. The acoustic impedance mismatch at the pipe outlet (open acoustic boundary condition) leads to plane wave reflection and hence the complex standing wave formation in a network. It is found that the acoustic eigenmodes is independent of the three-dimensional (3D) topology [31], while the structural eigenmodes are influenced by the 3D topology through stiffness distributions of clamped supports (see Section 4.2.1 and Fig. 4*d,e,f*).

4.2.1. Influence of support systems

The structural response of a piping beam network subjected to acoustic-induced shaking forces is highly influenced by the type and number of support systems. Using a parametric analysis by uniformly changing a longitudinal spring constant (k), we investigated the influence of varying the stiffness of the clamped supports (COMBIN14 elastic springs) on the structural eigenfrequencies (see Fig. 4*d,e,f*). The structural eigenfrequencies are relatively closely-spaced and well-separated when the piping network is supported with $k < 10^6$ N/m (see Fig. 4*d*) and $k \gg 10^6$ N/m (see Fig. 4*e,f*), respectively. During acoustic-structure coupling at resonance condition, the piping network with $k < 10^6$ N/m is more prone to energy exchange between two adjacent eigenmodes than $k \gg 10^6$ N/m, which can cause severe problems, such as the beating phenomenon. To avoid the coincidence of first pulsatile flow harmonics with one of the structural closely-spaced eigenfrequencies in the 20% resonance bandwidth in flexible piping networks ($k < 10^6$ N/m), we have chosen the support system with $k = 10^9$ N/m in our study. The eigenmodes separation becomes quasi-similar when $k = 10^9, 10^{12}$, and 10^{15} N/m.

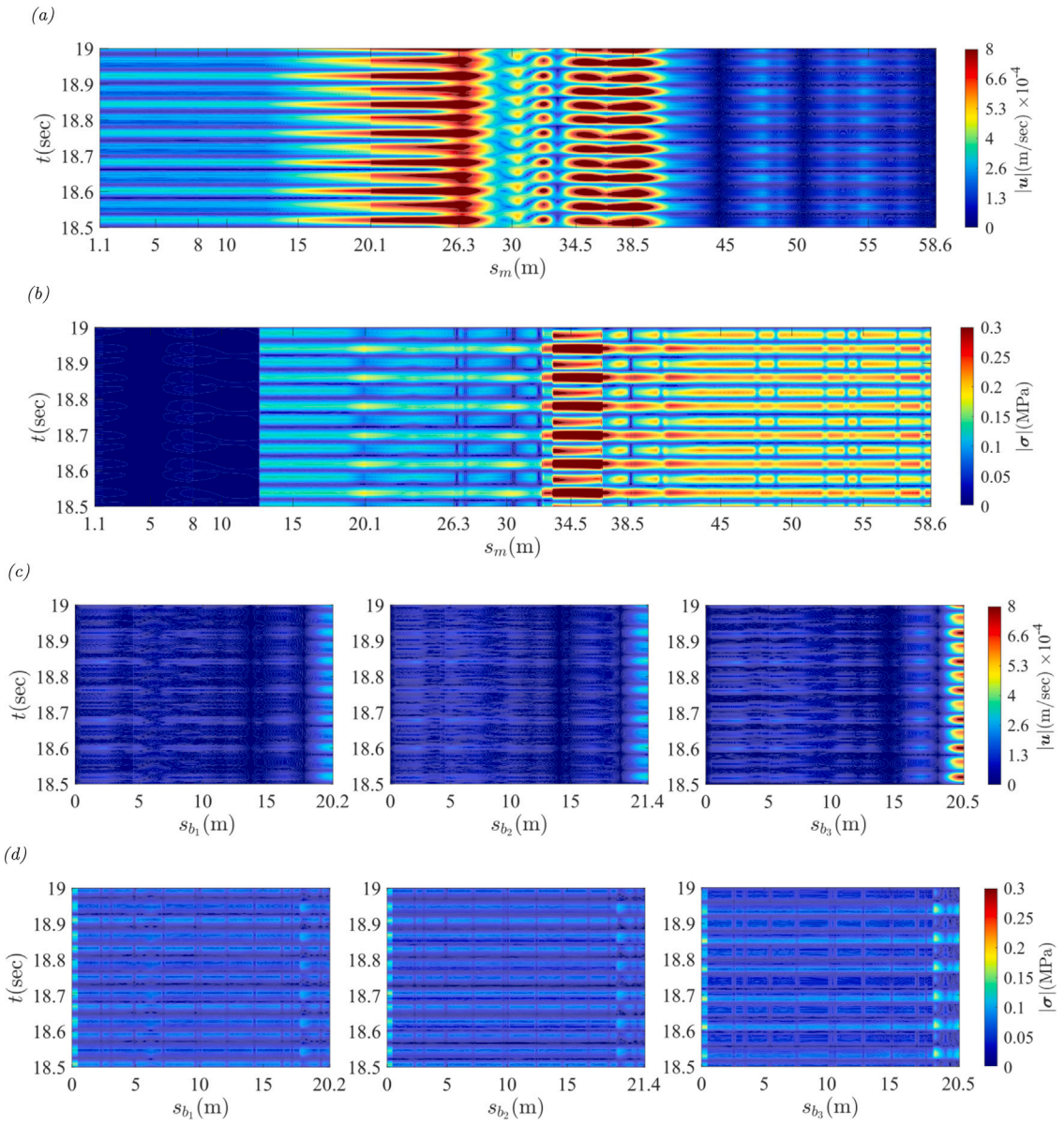

Fig. 6. Time-history diagrams showing the global distribution of (a, c) vibration-induced velocity $|\boldsymbol{u}|$ and (b, d) stress $|\boldsymbol{\sigma}|$ in a piping network (see Fig. 3*b*). The contour plots are shown separately for (a, b) mainline and (c, d) branch networks.

4.3. Pressure pulsation

In a piping system connected with pumps having $f_{p_r} = 5.77$ Hz and $\eta_v = 0.95$, acoustic wave responses are captured at the points of junction coupling. Only the responses at $s_m = 26.3$ m (see Fig. 3) are shown here. Fig. 5 shows the steady-state, transient-state, and combined steady-transient-state characteristics of plane acoustic wave propagation in a liquid-filled piping network (see Figs. 1 and 3*a*) due to pulsatile flow-acoustic interaction mechanisms associated with various pump loading operations (see Fig. 2).

4.3.1. Steady-state response

The pulsatile flow-acoustic interaction due to steady pump loading with pulsatile flows (see Fig. 2*a*) generates steady-state characteristics of plane acoustic waves with constant amplitude (see Fig. 5 and snapshot **C**). The pulsatile-flow-induced acoustic response with largest amplitude at first ($m_p = 1$) pulsatile flow harmonics $f_{m_p} = 1 \times 5 \times 5.77 = 26$ Hz is consistent with Fig. 4*c*.

4.3.2. Transient-state response

As a result of dynamic pump loading (rapid startup and shutdown) with mean flow, the piping network generates plane acoustic waves in the form of an oscillating pressure transient (see Fig. 5 and snapshot **A**). This pressure transient has similar characteristics to that of plane acoustic wave propagation in the presence of a centrifugal pump [3–5,72,73]. Flow transient predominately excites the fundamental acoustic eigenmode of a piping network [74] due to rapid accelerating and decelerating events, e.g., rapid opening and closure of discharge valve [74, Fig. 2*a*]. Similarly, the fundamental acoustic eigenmode at $f = 4.3$ Hz (see Fig. 4*c*) is significantly excited during the startup–shutdown events of dynamic pump loading. These startup and shutdown-induced transient pressure waves propagate along the network, initiating propagation from pipe inlets and then reflecting back at pipe outlets, causing standing waves to form.

The attenuation of transient-induced plane acoustic waves at startup and shutdown (see Fig. 5 and snapshot **A**) can be anticipated from the friction losses through various piping components (straight and fitting pipes) [31]. It is also worth noting that the transient-induced plane

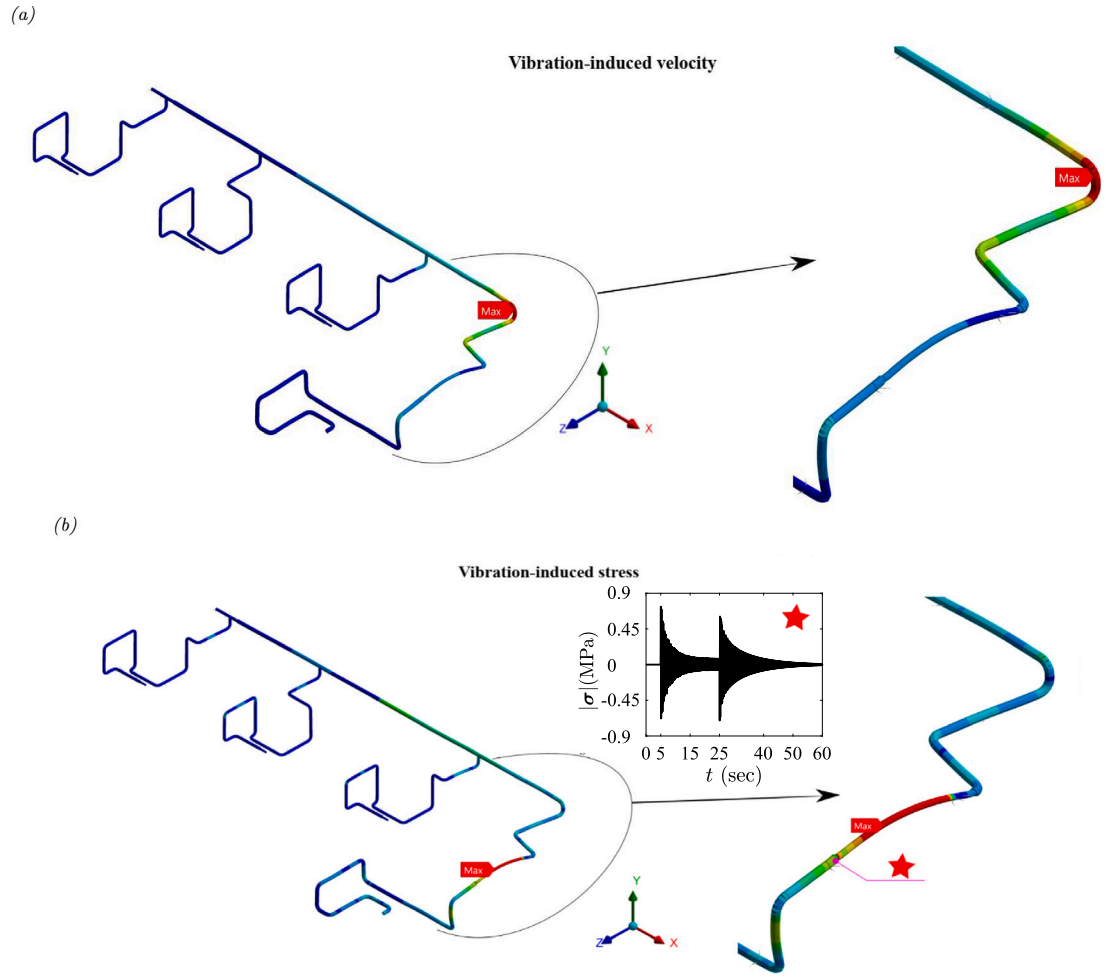

Fig. 7. Structural response in a piping network driven by dynamic pump loading with pulsatile flows. (*a,b*) Contour distribution of vibration-induced velocity and stress in a piping network, respectively. The enlarged contour plots on the right highlight the maximum velocity and Von-mises stress. The line plot in the inset of *b* shows the stress history at the fatigue sensitive critical location (red-star marker).

acoustic wave during startup attenuates faster than shut-down. The attenuation characteristics of transients associated with rapid pump startup and shutdown are similar to the transients due to rapid valve opening and closure [18] in reservoir–pipe–valve (RPV) system, respectively) [3–5].

4.3.3. *Combined steady-transient-state response*

The pump–acoustic interaction associated with steady pump loading with pulsatile flows and dynamic pump loading with the mean flow is stationary (same frequency component throughout time). On the other hand, the pump–acoustic interaction due to dynamic pump loading (startup–shutdown) with pulsatile flows (see Fig. 2) generates non-stationary plane acoustic waves (see Fig. 5; highlighted by snapshots **A** and **B**). The pump-flow-induced acoustic response is the superposition of high-amplitude low-frequency (based on fundamental acoustic eigenmode) transient characteristics of plane acoustic waves (snapshot **A**) and low-amplitude high-frequency (based on pump harmonics) steady characteristics of plane acoustic waves (snapshot **C**).

4.4. *Pulsation-induced vibration*

The two major consequences of the interaction of dynamic pump loading (startup–shutdown operation) with the acoustical and structural eigenmodes are the acoustic-induced shaking forces and vibration-induced stresses in a piping network. The acoustic–structural interaction causes energy exchange between acoustics and structures and hence leads to vibration in a piping network [7,8]. When a piping network contains multiple changes in the flow direction, it becomes susceptible to vibration caused by shaking forces that act at pipe bends and tees due to acoustic–structural coupling. The shaking forces are generated at pipe fittings due to the combined steady-state and transient characteristics of pressure pulsation. Various segments in a three-dimensional piping network are then subjected to a complex state of combined loading (tension/compression, bending, and torsion) due to junction coupling at bends and tees in the form of pump–acoustic–mechanical coupling. This leads to a generation of large piping vibration-induced velocity and vibration-induced stresses.

We utilise structural vibration analysis results to derive time-span diagrams that allow us to see structural vibration velocity and stress against piping longitudinal positions (shown also by [6,75]). Here, the times are plotted against piping longitudinal position with an overlay of vibration-induced velocity (**u**) and stress (σ) (see Fig. 6*a,c* and *b,d*, respectively). Using time-span diagram, the location of maximum velocity (at $s = 26.3$ m) and stress (at $s = 35$ m) can be easily identified and distinguished. Fig. 7(*a,b*) shows the global distribution of maximum vibration velocity and Von-mises stress in a piping network which is driven by dynamic pump loading with pulsatile flows (see Fig. 2*c*).

In the present study, we highlight the fundamental mechanisms underlying the influence of pumps starting and stopping dynamic loading on the coupled acoustic–structural response of a piping network. In practical systems, the pump operations include multiple startup–shutdown events during operation. The turbo-machineries can undergo

startup and shutdown operations under two scenarios: (a) the regular maintenance required to ensure smooth operation and (b) the emergency shutdown in case of a failure. Consequently, startup and shutdown transients are detrimental to machinery because of the intermittent operational cycles (startup and shutdown frequency), which can cause fatigue failure due to the interaction mechanism between low-cycle fatigue and high-cycle fatigue (LCF–HCF).

5. Summary and conclusion

The study highlights various contributions to the acoustic–structural coupling mechanisms in a complex piping network due to dynamic pump loading operations. The piping network is equipped with three reciprocating pumps, each generating three types of discharge flows, i.e., steady-state pump loading with pulsatile flows, dynamic pump loading with mean flows and dynamic pump loading with pulsatile flows. The MOC-FEM framework is applied to a typical rapid startup–shutdown operation of pumps generating pulsatile flows, which is not a feature of most of the piping pulsation–vibration assessment tools. The following conclusions can be drawn:

1. Transient-state characteristics of plane acoustic wave propagation are independent of pulsatile flow harmonics, whereas steady-state characteristics are driven by interactions between pulsatile flow harmonics and acoustic eigenmodes.
2. Transient-state acoustic resonances are observed at the fundamental eigenfrequency, which results in an increase in the pulsatile flow-induced acoustic pressure and acoustic-induced vibration stresses in piping networks.
3. Pump loading under dynamic conditions with pulsatile flows generates complex acoustic responses in a piping network, which produce an extremely different behaviour from that expected for pump loading under steady-state conditions. During the pump startup–shutdown event, the acoustic pressure is the superposition of moderate-to-high-frequency steady-state characteristics (with low amplitude) and the low-frequency transient characteristics (with large amplitude).
4. A recent study suggested that the attenuation in transient plane acoustic waves could be attributed to the pipe friction effect, which is caused by straight pipes and fittings.

A piping system's reliability and integrity depend on the systematic analysis of its structural responses during many transient cycles. As part of the future work, we will incorporate (multiple) daily startup–shutdown cycles and load variations into the fatigue assessment in order to quantify vibration-induced fatigue. This assessment will include a consideration of the interaction between low-cycle fatigue and high-cycle fatigue.

CRediT authorship contribution statement

Feroz Ahmed: Conceptualization, Methodology, Software, Investigation, Formal analysis, Visualization, Writing – original draft. **Ian Eames:** Supervision. **Alireza Azarbadegan:** Supervision, Resources. **Emad Moeendarbary:** Supervision, Funding acquisition, Project administration.

Declaration of competing interest

The authors declare that they have no known competing financial interests or personal relationships that could have appeared to influence the work reported in this paper.

Acknowledgements

A.A. acknowledges the support of Geoff Evans (BP) for this collaborative project. E.M. is grateful for financial support from the Biotechnology and Biological Sciences Research Council, UK (BB/V001418/1) and Engineering and Physical Research Council, UK (EP/W009889/1).

Funding

This work was supported by the UK Engineering and Physical Science Research Council (EPSRC) and British Petroleum (BP), *UK through Industrial Cooperative Awards in Science & Technology (iCASE), UK [Grant number EP/S513726/1, Ph.D. studentship project reference number 2309782].

References

[1] Afshar MH, Rohani M, Taheri R. Simulation of transient flow in pipeline systems due to load rejection and load acceptance by hydroelectric power plants. Int J Mech Sci 2010;52(1):103–15, URL https://doi.org/10.1016/j.ijmecsci.2009.10.014.

[2] Romuald B, Jian Z, Dong YX, Claire D. Assessment and performance evaluation of water hammer in hydroelectric plants with hydropneumatic tank and pressure regulating valve. J Press Vessel Technol 2021;143(4). URL https://doi.org/10.1115/1.4049148.

[3] Tanaka T, Tsukamoto H. Transient behavior of a cavitating centrifugal pump at rapid change in operating conditions—Part 1: Transient phenomena at opening/closure of discharge valve. J Fluids Eng 1999. URL https://doi.org/10.1115/1.2823545.

[4] Tanaka T, Tsukamoto H. Transient behavior of a cavitating centrifugal pump at rapid change in operating conditions—Part 2: Transient phenomena at pump startup/shutdown. J Fluids Eng 1999. URL https://doi.org/10.1115/1.2823546.

[5] Tanaka T, Tsukamoto H. Transient behavior of a cavitating centrifugal pump at rapid change in operating conditions—Part 3: Classifications of transient phenomena. J Fluids Eng 1999. URL https://doi.org/10.1115/1.2823547.

[6] Yan W, Hongkang D, Yongling HE. A novel approach for predicting inlet pressure of aircraft hydraulic pumps under transient conditions. Chin J Aeronaut 2019;32(11):2566–76, URL https://doi.org/10.1016/j.cja.2019.03.041.

[7] Miao Y, Jiang Y, Qiu Z, Pan J, Wang L, Han Z, Li K, Zhang L, Zhang X. Vibration transients of reservoir-pipe-valve system caused by water hammer. J Theor Appl Mech 2020;58. URL https://doi.org/10.15632/jtam-pl/127288.

[8] Miao Y, Qiu Z, Zhang X, Jiang Y, Pan J, Liu Y, Zhang L, Li K. Effects of a water hammer and cavitation on vibration transients in a reservoir-pipe-valve system. J Theor Appl Mech 2021;59. URL https://doi.org/10.15632/jtam-pl/141335.

[9] Brighenti A, Bittante F, Parrozzani R. Advanced simulation techniques. Hydro Eng 2009;14:103–6, URL https://www.researchgate.net/publication/298565128_Advanced_simulation_techiques.

[10] Miyashiro H. Water hammer analysis for pumps in parallel operation. Bull JSME 1962;5(19):479–84, URL https://doi.org/10.1299/jsme1958.5.479.

[11] Feng J, Ge Z, Zhang Y, Zhu G, Wu G, Lu J, Luo X. Numerical investigation on characteristics of transient process in centrifugal pumps during power failure. Renew Energy 2021;170:267–76, URL https://doi.org/10.1016/j.renene.2021.01.104.

[12] Stephenson D. Simple guide for design of air vessels for water hammer protection of pumping lines. J Hydraul Eng 2002;128(8):792–7, URL https://doi.org/10.1061/(ASCE)0733-9429(2002)128:8(792).

[13] Yang Z, Cheng Y, Xia L, Meng W, Liu K, Zhang X. Evolutions of flow patterns and pressure fluctuations in a prototype pump-turbine during the runaway transient process after pump-trip. Renew Energy 2020;152:1149–59, URL https://doi.org/10.1016/j.renene.2020.01.079.

[14] Duan HF, Tung YK, Ghidaoui MS. Probabilistic analysis of transient design for water supply systems. J Water Resour Plan Manage 2010;136(6):678–87, URL https://doi.org/10.1061/(ASCE)WR.1943-5452.0000074.

[15] Meniconi S, Brunone B, Ferrante M, Massari C. Potential of transient tests to diagnose real supply pipe systems: What can be done with a single extemporary test. J Water Resour Plan Manage 2011;137(2):238–41, URL https://doi.org/10.1061/(ASCE)WR.1943-5452.0000098.

[16] Meniconi S, Brunone B, Ferrante M, Capponi C, Carrettini CA, Chiesa C, Segalini D, Lanfranchi E. Anomaly pre-localization in distribution–transmission mains by pump trip: preliminary field tests in the milan pipe system. J Hydroinform 2015;17(3):377–89, URL https://doi.org/10.2166/hydro.2014.038.

[17] Ferras D, Manso PA, Schleiss AJ, Covas DIC. Fluid-structure interaction in straight pipelines with different anchoring conditions. J Sound Vib 2017;394:348–65, URL https://doi.org/10.1016/j.jsv.2017.01.047.

[18] Zouari F, Nasraoui S, Louati M, Ghidaoui MS. Transformation between damped and undamped waterhammer waves. J Sound Vib 2021;491:115706, URL https://doi.org/10.1016/j.jsv.2020.115706.

[19] Tsukamoto H, Ohashi H. Transient characteristics of a centrifugal pump during starting period. J Fluids Eng 1982. URL https://doi.org/10.1115/1.3240859.

[20] Saito S. The transient characteristics of a pump during start up. Bull JSME 1982;25(201):372–9, URL https://doi.org/10.1299/jsme1958.25.372.

[21] Tsukamoto H, Matsunaga S, Yoneda H, Hata S. Transient characteristics of a centrifugal pump during stopping period. J Fluids Eng 1986. URL https://doi.org/10.1115/1.3242594.

[22] Wan W, Li F. Sensitivity analysis of operational time differences for a pump–valve system on a water hammer response. J Press Vessel Technol 2016;138(1). URL https://doi.org/10.1115/1.4031202.

[23] Liang Z, Li S, Tian J, Zhang L, Feng C, Zhang L. Vibration cause analysis and elimination of reciprocating compressor inlet pipelines. Eng Fail Anal 2015;48:272–82, URL https://doi.org/10.1016/j.engfailanal.2014.11.003.

[24] Choy FK, Braun MJ, Wang HS. Transient pressure analysis in piping networks due to valve closing and outlet pressure pulsation. J Press Vessel Technol 1996. URL https://doi.org/10.1115/1.2842194.

[25] Zhang W, Yang S, Wu D, Xu Z. Dynamic interaction between valve-closure water hammer wave and centrifugal pump. Proc Inst Mech Eng C 2021;235(23):6767–81, URL https://doi.org/10.1177/09544062211000768.

[26] Ismaier A, Schlücker E. Fluid dynamic interaction between water hammer and centrifugal pumps. Nucl Eng Des 2009;239(12):3151–4, URL https://doi.org/10.1016/j.nucengdes.2009.08.028.

[27] Zarzycki Z, Kudźma S, Kudźma Z, Stosiak M. Simulation of transient flows in a hydraulic system with a long liquid line. J Theor Appl Mech 2007;45(4):853–71.

[28] Streeter VL, Wylie EB. Hydraulic transients caused by reciprocating pumps. J Eng Power 1967. URL http://dx.doi.org/10.1115/1.3616754.

[29] Dong J, Liu Y, Ji H, Wei L, Wu D. Simulation of unsteady flow characteristics of the reciprocating pump check valve for high pressure and high flow water medium. J Fluids Eng 2022;144(3). URL https://doi.org/10.1115/1.4052177.

[30] Pei J, He C, Lv M, Huang X, Shen K, Bi K. The valve motion characteristics of a reciprocating pump. Mech Syst Signal Proc 2016;66:657–64, URL https://doi.org/10.1016/j.ymssp.2015.06.013.

[31] Ahmed F, Eames I, Azarbadegan A, Moeendarbary E. Acoustics interaction in a complex piping network with multiple pulsatile sources. J Sound Vib 2022. URL https://doi.org/10.1016/j.jsv.2022.116863.

[32] Huang ZF. Transient modelling of a positive displacement pump for advanced power cycle applications (Bachelors thesis), 2017.

[33] Behroozi AM, Vaghefi M. Numerical investigation of water hammer due to transient in parallel pumps. Int J Civ Eng 2021;1–11, URL http://dx.doi.org/10.1007/s40999-021-00640-w.

[34] Gao P, Qu H, Zhang Y, Yu T, Zhai J. Experimental and numerical vibration analysis of hydraulic pipeline system under multiexcitations. Shock Vib 2020. URL https://doi.org/10.1155/2020/3598374.

[35] Tian W, Su GH, Wang G, Qiu S, Xiao Z. Numerical simulation and optimization on valve-induced water hammer characteristics for parallel pump feedwater system. Ann Nucl Energy 2008;35(12):2280–7, URL http://dx.doi.org/10.1016/j.anucene.2008.08.012.

[36] Feng T, Zhang D, Song P, Tian W, Li W, Su GH, Qiu S. Numerical research on water hammer phenomenon of parallel pump-valve system by coupling FLUENT with RELAP5. Ann Nucl Energy 2017;109:318–26, URL https://doi.org/10.1016/j.anucene.2017.05.049.

[37] Gao P, Zhang Y, Liu X, Yu T, Wang J. Vibration analysis of aero parallel-pipeline systems based on a novel reduced order modeling method. J Mech Sci Technol 2020;34(8):3137–46, URL http://dx.doi.org/10.1007/s12206-020-0705-3.

[38] Manring ND. The discharge flow ripple of an axial-piston swash-plate type hydrostatic pump. J Dyn Syst Meas Control 2000;122(2):263–8, URL https://doi.org/10.1115/1.482452.

[39] Josifovic A, Corney J, Davies B. Valve dynamics in multi-cylinder positive displacement pump model. In: 2015 IEEE intl. conf. advanced intelligent mechatronics. IEEE; 2015, p. 35–41, URL https://doi.org/10.1109/AIM.2015.7222505.

[40] Kita Y, Adachi Y, Hirose K. Periodically oscillating turbulent flow in a pipe. JSME Bull 1980;23(179):656–64, URL https://doi.org/10.1299/jsme1958.23.656.

[41] Mao ZX, Hanratty TJ. Studies of the wall shear stress in a turbulent pulsating pipe flow. J Fluid Mech 1986;170:545–64, URL https://doi.org/10.1017/S0022112086001015.

[42] Zielke W. Frequency-dependent friction in transient pipe flow. Trans ASME J Basic Eng 1968;90(1):109–15, URL https://doi.org/10.1115/1.3605049.

[43] Vardy AE, Brown JM. Transient turbulent friction in smooth pipe flows. J Sound Vib 2003;259(5):1011–36, URL https://doi.org/10.1006/jsvi.2002.5160.

[44] Vardy AE, Brown JM. Transient turbulent friction in fully rough pipe flows. J Sound Vib 2004;270(1–2):233–57, URL https://doi.org/10.1016/S0022-460X(03)00492-9.

[45] D'Souza AF. Dynamic response of fluid flow through straight and curved lines (Masters thesis), Purdue University; 1963.

[46] Vardy AE, Brown JMB. Transient, turbulent, smooth pipe friction. J Hydraul Res 1995;33(4):435–56, URL https://doi.org/10.1080/00221689509498654.

[47] Vardy AE, Brown JM. Approximation of turbulent wall shear stresses in highly transient pipe flows. J Hydraul Eng 2007;133(11):1219–28, URL https://doi.org/10.1061/(ASCE)0733-9429(2007)133:11(1219).

[48] Duan HF, Che TC, Lee PJ, Ghidaoui MS. Influence of nonlinear turbulent friction on the system frequency response in transient pipe flow modelling and analysis. J Hydraul Res 2018;56(4):451–63, URL https://doi.org/10.1080/00221686.2017.1399936.

[49] Duan HF, Ghidaoui MS, Lee PJ, Tung YK. Relevance of unsteady friction to pipe size and length in pipe fluid transients. J Hydraul Eng 2012;138(2):154–66, URL http://dx.doi.org/10.1061/(ASCE)HY.1943-7900.0000497.

[50] Duan HF, Meniconi S, Lee PJ, Brunone B, Ghidaoui MS. Local and integral energy-based evaluation for the unsteady friction relevance in transient pipe flows. J Hydraul Eng 2017;143(7):04017015, URL http://dx.doi.org/10.1061/(ASCE)HY.1943-7900.0001304.

[51] Ahmed F, Eames I, Moeendarbary E, Azarbadegan A. High-strouhal-number pulsatile flow in a curved pipe. J Fluid Mech 2021;923. URL https://doi.org/10.1017/jfm.2021.553.

[52] Ghidaoui MS, Zhao M, Mcinnis DA, Axworthy DH. A review of water hammer theory and practice. Appl Mech Rev 2005;58(1):49–76, URL https://doi.org/10.1115/1.1828050.

[53] Bergant A, Simpson A, Vitkovsky J. Review of unsteady friction models in transient pipe flow. In: The Behaviour of Hydraulic Machinery Under Steady Oscillatory Conditions. IAHR Work Group, Ninth International Meeting, 7–9 September, Brno, Czech Republic; 1999.

[54] Timoshenko SP. LXVI. On the correction for shear of the differential equation for transverse vibrations of prismatic bars. Lond Edinb Dublin Philos Mag J Sci 1921;41(245):744–6, URL https://doi.org/10.1080/14786442108636264.

[55] Reissner E. The effect of transverse shear deformation on the bending of elastic plates. J Appl Mech ASME 1945. URL https://doi.org/10.1115/1.4009435.

[56] Mindlin RD. Influence of rotatory inertia and shear on flexural motions of isotropic, elastic plates. J Appl Mech ASME 1951. URL https://doi.org/10.1115/1.4010217.

[57] Wiggert DC. Coupled transient flow and structural motion in liquid-filled piping systems: a survey. In: Proc. ASME pres. ves. piping conf., Vol. 25, Chicago, USA; 1986.

[58] Wiggert DC. Fluid transients in flexible piping systems. In: Hyd. mach. cavitation. Springer; 1996, p. 58–67.

[59] Tijsseling AS. Fluid-structure interaction in liquid-filled pipe systems: a review. J Fluids Struct 1996;10(2):109–46, URL https://doi.org/10.1006/jfls.1996.0009.

[60] Wiggert DC, Tijsseling AS. Fluid transients and fluid-structure interaction in flexible liquid-filled piping. Appl Mech Rev 2001;54(5):455–81, URL https://doi.org/10.1115/1.1404122.

[61] Li S, Karney BW, Liu G. FSI research in pipeline systems–a review of the literature. J Fluids Struct 2015;57:277–97, URL https://doi.org/10.1016/j.jfluidstructs.2015.06.020.

[62] Ferras D, Manso PA, Schleiss AJ, Covas DIC. One-dimensional fluid–structure interaction models in pressurized fluid-filled pipes: A review. Appl Sci 2018;8(10):1844, URL https://doi.org/10.3390/app8101844.

[63] Lavooij CSW, Tusseling AS. Fluid-structure interaction in liquid-filled piping systems. J Fluids Struct 1991;5(5):573–95, URL https://doi.org/10.1016/S0889-9746(05)80006-4.

[64] Ahmadi A, Keramat A. Investigation of fluid–structure interaction with various types of junction coupling. J Fluids Struct 2010;26(7–8):1123–41, URL http://dx.doi.org/10.1016/j.jfluidstructs.2010.08.002.

[65] Aliabadi HK, Ahmadi A, Keramat A. Frequency response of water hammer with fluid-structure interaction in a viscoelastic pipe. Mech Syst Signal Process 2020;144:106848, URL https://ui.adsabs.harvard.edu/link_gateway/2020MSSP..14406848A/doi:10.1016/j.ymssp.2020.106848.

[66] Sreejith B, Jayaraj K, Ganesan N, Padmanabhan C, Chellapandi P, Selvaraj P. Finite element analysis of fluid–structure interaction in pipeline systems. Nucl Eng Des 2004;227(3):313–22, URL http://dx.doi.org/10.1016/j.nucengdes.2003.11.005.

[67] Zhang YL, Gorman DG, Reese JM. A finite element method for modelling the vibration of initially tensioned thin-walled orthotropic cylindrical tubes conveying fluid. J Sound Vib 2001;245(1):93–112, URL http://dx.doi.org/10.1006/JSVI.2000.3554.

[68] Cao H, Mohareb M, Nistor I. Finite element for the dynamic analysis of pipes subjected to water hammer. J Fluids Struct 2020;93:102845, URL https://doi.org/10.1016/j.jfluidstructs.2019.102845.

[69] Zanganeh R, Jabbari E, Tijsseling A, Keramat A. Fluid-structure interaction in transient-based extended defect detection of pipe walls. J Hydraul Eng 2020;146(4):04020015, URL https://doi.org/10.1061/(ASCE)HY.1943-7900.0001693.

[70] Oinonen A. Water hammer and harmonic excitation response with fluid-structure interaction in elbow piping. J Press Vessel Technol 2022;144(3). URL https://doi.org/10.1115/1.4051107.

[71] Gao H, Guo C, Quan L. Fluid-structure interaction analysis of aircraft hydraulic pipe with complex constraints based on discrete time transfer matrix method. Appl Sci 2021;11(24):11918, URL https://doi.org/10.3390/app112411918.

[72] Elaoud S, Hadj TE. Influence of pump starting times on transient flows in pipes. Nucl Eng Des 2011;241(9):3624–31, URL https://doi.org/10.1016/j.nucengdes.2011.07.039.

[73] Omri F, Hadj TL, Elaoud S. Numerical study on the transient behavior of a radial pump during starting time. AQUA—Water Infrastruct Ecosyst Soc 2021;70(3):257–73, URL https://doi.org/10.2166/aqua.2021.136.

[74] Lee PJ, Duan H, Ghidaoui M, Karney B. Frequency domain analysis of pipe fluid transient behaviour. J Hydraul Res 2013;51(6):609–22, URL https://doi.org/10.1080/00221686.2013.814597.

[75] Xiong FR, Lan B. Cooperative design and optimization of reactor coolant system piping supports under static and dynamical load conditions. In: ASME pressure vessels piping conf.. 2018, URL https://doi.org/10.1115/PVP2018-84026.